Density fluctuations in liquid argon. II. Coherent dynamic structure factor at large wave numbers

A. A. van Well and L. A. de Graaf
Interuniversitair Reactor Instituut, 2629 JB, Delft, The Netherlands
(Received 21 May 1985)

Experimental results of the coherent dynamic structure factor $S(k,\omega)$, obtained by inelastic neutron scattering, are presented for liquid argon at three densities along the 120-K isotherm. The wave numbers k, covered by the experiment, range from 38 to 72 nm^{-1}. The transition of $S(k,\omega)$ to its free-gas behavior (the limit for $k\rightarrow\infty$) is compared with theoretical calculations. It appears that the experimental results can be described satisfactorily by theoretical calculations for a Lennard-Jones system, whereas the large-k expansion for a hard-spheres system fails to describe the present argon results.

I. INTRODUCTION

In recent years[1,2] we reported the coherent dynamic structure factor $S(k,\omega)$ of liquid argon along the 120-K isotherm at pressures ranging from 2 to 85 MPa, obtained by means of inelastic neutron scattering (INS). These experiments covered a wave-number range of $4\lesssim k\lesssim 40$ nm^{-1}. Here, we present experimental $S(k,\omega)$ results of liquid argon (^{36}Ar) at 120 K and 2, 27, and 40 MPa in the wave-number range $38<k<72$ nm^{-1}. The aim of this extension to larger k values is to investigate the transition to the free-gas limit.

The large-k behavior of $S(k,\omega)$ has been the subject of earlier studies. Nijboer and Rahman[3] derived a large-k series expansion, with small parameter k^{-2}, for the incoherent (self) part of the dynamic structure factor, $S_s(k,\omega)$, for a classical system in the Gaussian approximation. In this approximation the assumption is made that the Fourier transform of $S_s(k,\omega)$, the intermediate scattering function $F_s(k,t)$, can be written as $F_s(k,t)=\exp[-k^2\gamma(t)]$, where the width function $\gamma(t)$ is proportional to the mean-square displacement of a single particle.

Sears[4] derived an exact large-k expansion of $S_s(k,\omega)$ for a classical system with particles interacting via a smooth velocity-independent interaction potential, yielding the same leading correction term (order k^{-2}) as in Nijboer and Rahman's description. For a quantum system Sears[5] derived a similar expansion which is correct in the Gaussian approximation.

For the total (coherent) $S(k,\omega)$ a large-k expansion is not possible due to its oscillating character as a function of k. Both for a classical[3] and a quantum[5] system, at fixed k, $S(k,\omega)$ can be expressed in a Gram-Charlier (GC) series expansion. This is a series in terms of Hermite polynomials in ω where the coefficients are determined by the frequency moments of $S(k,\omega)$. Although this is not a strict large-k expansion, it is expected to give a good approximation for large k since it was derived from a short-time expansion of $F(k,t)$. Truncation of this GC series after the fourth-order term [this is the order which gives the leading correction term, of order k^{-2}, in the classical case for $S_s(k,\omega)$], led to a qualitatively correct description of the experimental results for liquid neon[5] and liquid ^{4}He (Ref. 6) at large k.

The outline of this paper is as follows. In Sec. II the the neutron scattering experiment is described and some details of the necessary corrections are discussed. In Sec. III we present the resulting data. In Sec. IV the symmetrized (quasiclassical) experimental $S(k,\omega)$ data are compared with the classical version of the GC expansion. Furthermore the peak position of the measured, not symmetrized, $S(k,\omega)$ is compared with the quantum version of the GC expansion. Our conclusions are summarized in Sec. V.

II. EXPERIMENT

A. Measurements

Thermal neutron time-of-flight (TOF) spectra were obtained with the rotating-crystal spectrometer RKS II (Ref. 7) at the Interuniversitair Reactor Instituut (IRI) in Delft. The wavelength of the monochromatic beam was selected by reflection at a Bragg angle of $\theta_B=58.9(3)°$ from the (0 0 8) planes of a pyrolytic graphite (PG) crystal, yielding a wavelength $\lambda_0=0.1436(5)$ nm, corresponding to an energy $E_0=39.7(3)$ meV. Reflections from other lattice planes were suppressed by two choppers, rotating in phase with the PG monochromator. The dimensions of the monochromatic beam were 100×25 mm^2. The 36 ^{3}He detectors, positioned at 1.447 m from the sample, were combined to 15 detector groups. The first seven groups contained 23 detectors of 20 cm length, 1.27 cm diameter, and 10 bar filling pressure, and covered a scattering angle range of $48.8°<\varphi<81.8°$. The remaining eight groups, with 13 detectors of 20 cm length, 2.54 cm diameter, and 4 bar filling pressure, covered the range $85.7°<\varphi<114.3°$. The detectors were placed in such a way as to minimize the intensity measured from the Bragg reflections by the aluminum sample container and by the windows of the cryostat. The kinematic region covered is shown in Fig. 1(a).

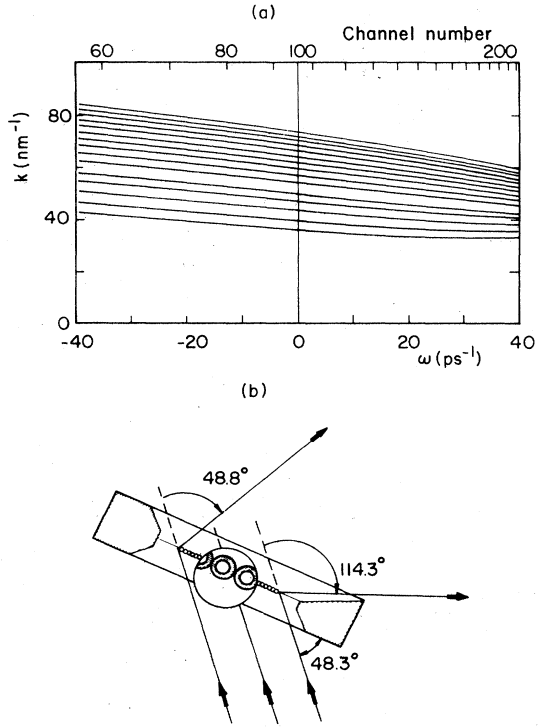

FIG. 1. (a) Kinematic region covered in the experiment: k as a function ω of the 15 experimental scattering angles. (b) Experimental scattering geometry.

The TOF system was triggered twice per revolution of the PG crystal, the time between two trigger pulses being 2400 μs. The spectra were recorded into 256 TOF channels 3 μs wide. The TOF resolution increased monotonically from 3.6% at the smallest scattering angle to 4.4% at the largest one, resulting in an absolute frequency resolution—for elastic scattering—of $4.2<\Delta\omega<5.3$ ps^{-1}. The ^{36}Ar sample and its container[8] were the same as described in Ref. 2. A part of the container frame was removed in order to allow for the use of the larger scattering angles. The scattering geometry is shown in Fig. 1(b).

Measurements on ^{36}Ar were performed at three thermodynamic conditions. The measured temperature T and pressure p, and the corresponding number density n (Ref. 9) are listed in Table I. Each measurement lasted for about 200 h resulting in a scattering intensity, integrated over all scattering angles and all TOF channels, of 3.5×10^6 counts [44%, 31%, and 25% emanating from ^{36}Ar, empty container (plus cryostat) scattering, and constant background, respectively]. Furthermore, we performed an empty container and a calibration measurement. For the latter we removed the container tubes and inserted a vanadium plate, 39 mm wide and 1.8 mm thick, in the frame. In this way, the same scattering geometry for all measurements was ensured. The samples were placed in a liquid-N_2 cryostat. The temperature of measurements I–IV was kept a 120 K (Table I). Measurement V was performed at 80 K in order to reduce the inelastic scattering intensity by the vanadium. At 80 K the contribution of this scattering is given by $1-\exp(-ak^2)$ with $a=3.0\times10^{-5}$ nm^2,[10] yielding an inelastic fraction of 16% at the largest scattering angle. An empty frame measurement was run to determine the vanadium background.

TABLE I. Experimental conditions.

	Measurement	T (K)	P (MPa)	n (nm^{-3})
I:	^{36}Ar	119.99(6)	1.95(10)	17.59(7)
II:	^{36}Ar	120.10(5)	26.6(1)	19.48(4)
III:	^{36}Ar	120.06(12)	40.2(8)	20.14(4)
IV:	Empty container	120.0		
V:	Vanadium	80.0		70.9
VI:	V background	80.0		

B. Data reduction

The raw TOF spectra were corrected for background scattering, multiple scattering, duty-cycle overlap, detector efficiency, TOF resolution, and self-shielding. They were normalized absolutely and converted to $S(k,\omega)$ at a rectangular (k,ω) grid. The procedure followed was similar to the one described in Ref. 2. Use has been made of the routines discussed in Ref. 11.

As an input kernel for the multiple scattering correction we used the experimental $S(k,\omega)$ results from Ref. 2 for $k<40$ nm^{-1} and the GC expansion[3] (up to the fourth order) for $k>40$ nm^{-1}. Inputs for this model are the static structure factor $S(k)$, the pair correlation function $g(r)$, and the two-particle interaction potential $\varphi(r)$ (see Sec. IV). We calculated these functions for a system interacting via the Lennard-Jones (LJ) potential

$$\varphi(r)=4\varepsilon[(r/\sigma)^{-12}-(r/\sigma)^{-6}]\,, \tag{1}$$

with parameters $\sigma=0.336$ nm and $\varepsilon/k_B=123.3$ K,[12] with k_B Boltzmann's constant, according to the mean spherical approximation (MSA).[13] A second interaction step for this correction[2] was performed but did not alter the results significantly.

In the data-correction procedure we still had to deal with a small intensity arising from parasitic reflections from the PG crystal which were not completely suppressed by the choppers. We corrected for this intensity, which was most pronounced in the neutron energy-gain wing of the spectra, as described in Appendix A. In this appendix we also discuss the correction of the vanadium spectra for inelastic scattering.

The fully corrected TOF spectra were converted to $S(k,\omega)$, where k and ω are the momentum and energy in units of $\hbar$, respectively, which were transferred from the neutron to the liquid in the scattering process. Due to uncertainties (of the order of a few percent) in the volumes of both the argon and the vanadium sample, exposed to the incoming neutrons, the values of the corrected data were absolute except for one factor, close to unity. The data were renormalized by this factor, which was determined by comparing $S(k)=\int S(k,\omega)d\omega$, obtained from

the present data, with neutron diffraction results of neon[14] at corresponding thermodynamic conditions. For the scaling of T, n, and k we used as LJ parameters for neon[12] $\sigma=0.279$ nm^{-1} and $\varepsilon/k_B=36.2$ K.

The final $\tilde{S}(k,\omega)$ (symmetrized dynamic structure factor) results of all three measurements are tabulated in Ref. 15, with the quasiclassical approximation of $S(k,\omega)$ (Ref. 16) given by

$$\tilde{S}(k,\omega)=\exp\left[-\tfrac{1}{2}\beta\hbar\omega+\frac{\hbar^2k^2\beta}{8M}\right]S(k,\omega)\ , \tag{2}$$

with $\beta=(k_BT)^{-1}$, T the temperature, and M the mass of an ^{36}Ar particle ($M=59.73\times10^{-27}$ kg), which is symmetric in ω due to the detailed-balance condition

$$S(k,\omega)=\exp(\beta\hbar\omega)S(k,-\omega)\ . \tag{3}$$

We will use two rigorous relationships to check the quality of the corrected data: (i) the detailed-balance condition, Eq. (3), and (ii) the first frequency moment of $S(k,\omega)$,

$$\int_{-\infty}^{\infty}\omega S(k,\omega)d\omega=\omega_R=\hbar k^2/2M\ , \tag{4}$$

where $\hbar\omega_R$ is the recoil energy.

The detailed-balance condition implies that $\tilde{S}(k,\omega)$ is symmetric in ω. In Fig. 2 we show experimental $\tilde{S}(k,\omega)$ data extracted from both neutron energy-gain ($\omega<0$) and energy-loss ($\omega>0$) processes for measurement III at some representative ω values. The consistency between positive and negative ω data is quantified by the quality factor $Q(\omega)$.[11,2] If these data were uncorrelated and the loss and gain data were normally distributed around the same mean, $Q(\omega)$ would follow a χ^2 distribution with one degree of freedom and its expectation value would be 1. $Q(\omega)$ is displayed in Fig. 3(a) for all three measurements.

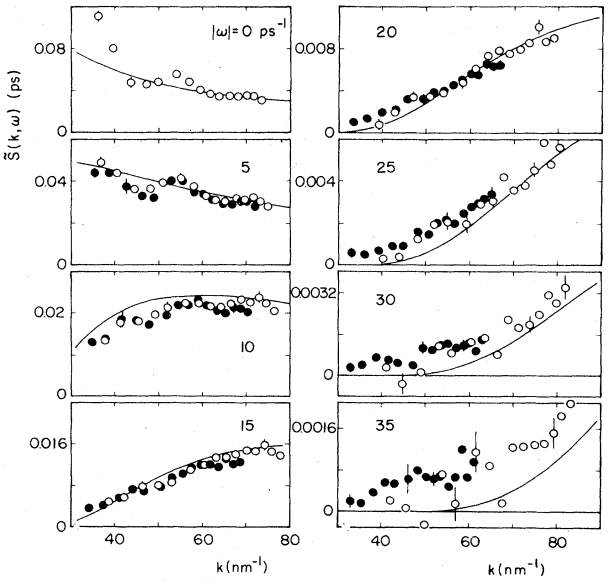

FIG. 2. Symmetrized dynamic structure factor $\tilde{S}(k,\omega)$ of measurement III as a function of k: neutron energy-loss data ($\omega<0$), open circles; energy-gain data ($\omega>0$), closed circles. Free-gas limit (at $T=122$ K) is represented by the solid lines.

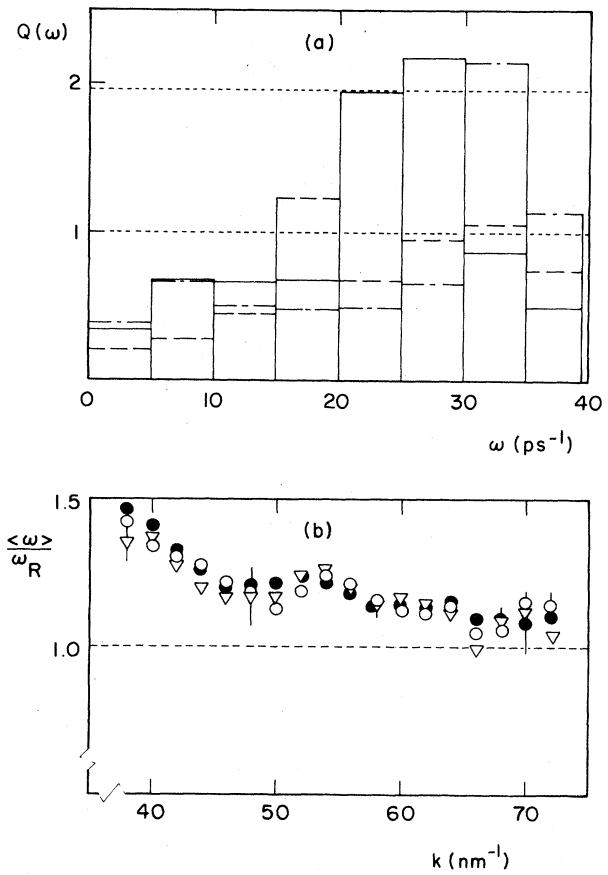

FIG. 3. (a) Quality factor $Q(\omega)$ for measurement I (solid line), II (dashed line), and III (dash-dotted line). Upper 95% limit and the mean of the χ^2 distribution with one degree of freedom are indicated by dotted lines. (b) Ratio of the experimental and theoretical first frequency moments for measurement I (closed circles), II (triangles), and III (open circles).

From Fig. 2 and Fig. 3(a) it is apparent that the energy-gain and energy-loss data agree satisfactorily, except for a small frequency range around 25 ps^{-1} in measurement I and around 30 ps^{-1} in measurement III.

The experimental first frequency moment of $S(k,\omega)$ divided by its theoretical value, $\langle\omega\rangle/\omega_R$, is shown in Fig. 3(b) as a function of k for all three measurements. For the calculation of $\langle\omega\rangle$ the experimental data were extrapolated, for $\omega>35$ ps^{-1}, by a Gaussian function.[11] Its width and amplitude were determined by a fit to the data in the range $17<\omega<35$ ps^{-1}, at fixed k. The contribution of this extrapolation to $\langle\omega\rangle$ was less than 3% for all k. Over the whole k range, $\langle\omega\rangle$ is too high. The origin of this enhancement may be found in imperfections in the correction for the parasitic reflections from the PG crystal, since the distortion of the spectra by these reflections is most serious in the far wings which considerably contribute to $\langle\omega\rangle$.

In a small-k region around $k=38$ nm^{-1} the present measurements and the ones reported in Ref. 2 overlap. Figure 4 shows $\tilde{S}(k,\omega)$ of ^{36}Ar at 120 K and 27 MPa from both sets. Regarding the estimated uncertainties the

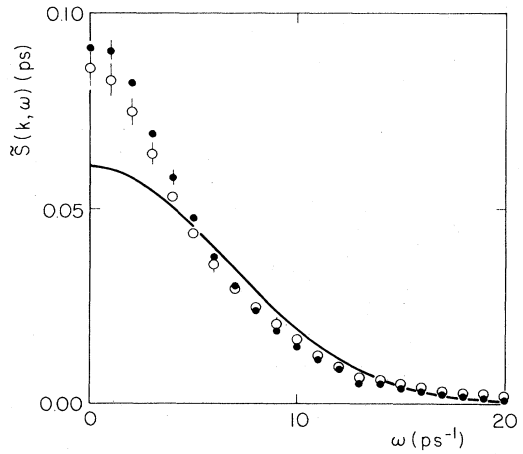

FIG. 4. $\widetilde{S}(k,\omega)$ at $k=39$ nm^{-1} of ^{36}Ar at 120 K and 27 MPa. Present results measurement II, open circles; Ref. 2 measurement *b*, closed circles; free-gas limit, solid line.

consistency is satisfactory. However, the shape of $\widetilde{S}(k,\omega)$ as a function of ω from Ref. 2 appears to be systematically somewhat sharper than that of the present $\widetilde{S}(k,\omega)$, which may indicate that at the smaller scattering angles in the latter case some resolution broadening is still left after the applied resolution correction (at the smallest scattering angle the width of the corrected argon spectrum was twice the width of the resolution function).

III. DYNAMIC STRUCTURE FACTOR

The large-k limit of $S(k,\omega)$ is given by the impulse approximation[5]

$$\lim_{k\to\infty} S(k,\omega)=S_{\mathrm{IA}}(k,\omega)=\int p(\mathbf{v})\delta(\omega-\omega_R-\mathbf{k}\cdot\mathbf{v})d\mathbf{v}\ , \quad (5)$$

where the δ function represents the conservation of momentum and energy during the collision of a neutron with an atom which has initially a velocity $\mathbf{v}$, and $p(\mathbf{v})$ is the normalized velocity distribution function. For a classical system in thermodynamic equilibrium at temperature T, $p(\mathbf{v})$ is given by the Maxwellian velocity distribution

$$p(\mathbf{v})=(2\pi v_0^2)^{-3/2}\exp\left[-\frac{v^2}{2v_0^2}\right] \quad (6)$$

with thermal velocity $v_0^2=(\beta M)^{-1}=k_BT/M$, yielding

$$S_{\mathrm{IA}}(k,\omega)=\frac{1}{\sqrt{2\pi}}\frac{1}{v_0k}\exp\left[-\frac{(\omega-\omega_R)^2}{2(v_0k)^2}\right]. \quad (7)$$

When first-order quantum effects (of order $\hbar^2$) are taken into account the velocity distribution remains Gaussian but the value of the thermal velocity increases.[17] In this approximation the system can still be considered a classical system having an effective temperature T_{eff} and a thermal velocity u given by

$$u^2=\frac{k_BT_{\mathrm{eff}}}{M}=v_0^2\left[1+\frac{\hbar^2\beta^2\Omega^2(0)}{12}\right], \quad (8)$$

with $\Omega^2(0)=(3M)^{-1}\langle\Delta V\rangle$. Here $\langle\Delta V\rangle$ is the classical equilibrium value of the Laplacian of the potential energy V. For a system with pairwise additive two-particle interaction potentials, $V=\frac{1}{2}\sum_{i,j}\varphi(|\mathbf{r}_i-\mathbf{r}_j|)$,

$$\Omega^2(0)=\frac{n}{M}\int g(r)\frac{d^2\varphi(r)}{dz^2}d\mathbf{r}\ . \quad (9)$$

The quasiclassical approximation of Eq. (2) adapted to $S_{\mathrm{IA}}(k,\omega)$ given by Eq. (7) results, to order $\hbar^2$, in the free-gas limit for a classical system with temperature T_{eff},

$$\widetilde{S}_{\mathrm{IA}}(k,\omega)\approx S_f(k,\omega)=\frac{1}{\sqrt{2\pi}}\frac{1}{uk}\exp\left[\frac{\omega^2}{2(uk)^2}\right], \quad (10)$$

where u is given by Eq. (8).

The effective temperature T_{eff} for the present experimental conditions, where the corrections are calculated for a LJ system according to the MSA,[13] is listed in Table II. The latter shows that $\Omega^2(0)$ as calculated is in excellent agreement with results from computer molecular-dynamics (CMD) simulations reported by Verlet.[18] In Ref. 2 it was shown that the MSA, adapted to a LJ system in the liquid phase, can very well describe the experimentally determined static structure factor $S(k)$ and the

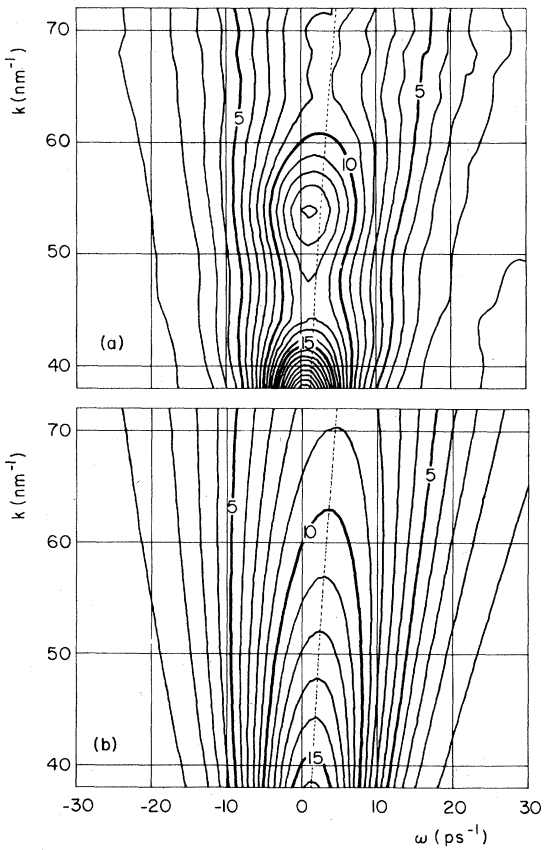

FIG. 5. Contour plot of (a) $S(k,\omega)$ of measurement III and (b) $S_{\mathrm{IA}}(k,\omega)$ [Eq. (7)]. Contour number i represents $S(k,\omega)=0.002+(i-1)0.004$ ps. Dotted curves indicate the recoil frequency $\omega_R=\hbar k^2/2M$.

TABLE II. Effective temperature, thermal velocity, [thermal velocity at $T=120$ K is $v_0=(\beta M)^{-1/2}=166.6$ ms^{-1}] and parameters in the Gram-Charlier expansion.

Experimental condition	$[\Omega^2(0)]^*$[a] MSA	Ref. 18[b]	T_{eff} (K)	u (ms^{-1})	k_1 (nm^{-1})	k_3 (nm^{-1})	k_4 (nm^{-1})
I	186	185	121.9	167.9	134	4.22	16.8
II	230	227	122.4	168.3	135	5.22	18.7
III	246	241	122.6	168.4	135	5.59	19.3

[a] $[\Omega^2(0)]^*=\Omega^2(0)\tau^2$, with $\tau=\sigma(M/\varepsilon)^{1/2}=1.99$ ps.
[b] From CMD using the interpolation formula $[\Omega^2(0)]^*=420(n^*)^2(T^*)^{1/2}$.

fourth frequency moment of $\tilde{S}(k,\omega)$.

For the comparison of the experimental symmetrized dynamic structure factor $\tilde{S}(k,\omega)$ with the free-gas limit $S_f(k,\omega)$ or with a classical theory, we will consider a classical system with temperature $T=122$ K in the remainder of this paper.

In Fig. 5(a) the $S(k,\omega)$ results of measurement III are displayed in a contour plot representation. For comparison, the large-k limit $S_{\text{IA}}(k,\omega)$—cf. Eq. (7) for a system with $T_{\text{eff}}=122$ K—is given in Fig. 5(b). Comparing Figs. 5(a) and 5(b) leads to the following observations. (i) The largest deviations of $S(k,\omega)$ from $S_{\text{IA}}(k,\omega)$ are found at small ω values. While $S_{\text{IA}}(k,\omega)$ exhibits a smooth and monotonic behavior a clear structure (with maxima near $k\approx 35$ and 55 nm^{-1}) is manifest in $S(k,\omega)$. (ii) Both at large ω and at large k, $S(k,\omega)$ goes over smoothly into $S_{\text{IA}}(k,\omega)$. (iii) At fixed k, $S_{\text{IA}}(k,\omega)$ is symmetric around the recoil frequency $\omega_R=\hbar k^2/2M$, where it has its maximum. However, at fixed k, $S(k,\omega)$ has its maximum at ω_p in between $\omega=0$ and ω_R (see Sec. IV B), and in the wings $S(k,\omega)>S(k,-\omega)$.

In Fig. 6 the deviation of the experimental symmetrized dynamic structure factor $\tilde{S}(k,\omega)$ from the free-gas limit $S_f(k,\omega)$,

$$\Delta S(k,\omega)=\frac{\tilde{S}(k,\omega)}{S(k)}-S_f(k,\omega)\ , \tag{11}$$

is shown, where $S(k)$ is the static structure factor obtained by numerical integration of $S(k,\omega)$ [within the estimated uncertainty, $S(k)$ determined from $S(k,\omega)$ was identical to $S(k)$ determined from $\tilde{S}(k,\omega)$]. By definition the area under $\Delta S(k,\omega)$ is equal to zero. At all k, $\Delta S(k,\omega)$ is positive at $\omega=0$. With increasing ω, $\Delta S(k,\omega)$ becomes negative, has a minimum at ω_{min}, becomes positive again at $\omega\sim 2\omega_{\text{min}}$, and then approaches zero.

In Fig. 7 $S(k)$ in the range $38<k<72$ nm^{-1}, determined from all three measurements, are shown together with $S(k)$, calculated according to the MSA (Ref. 13) and from a CMD simulation, both for a LJ system. We also show neutron diffraction (ND) data of neon at corresponding thermodynamic states.[14] The reduced tempera-

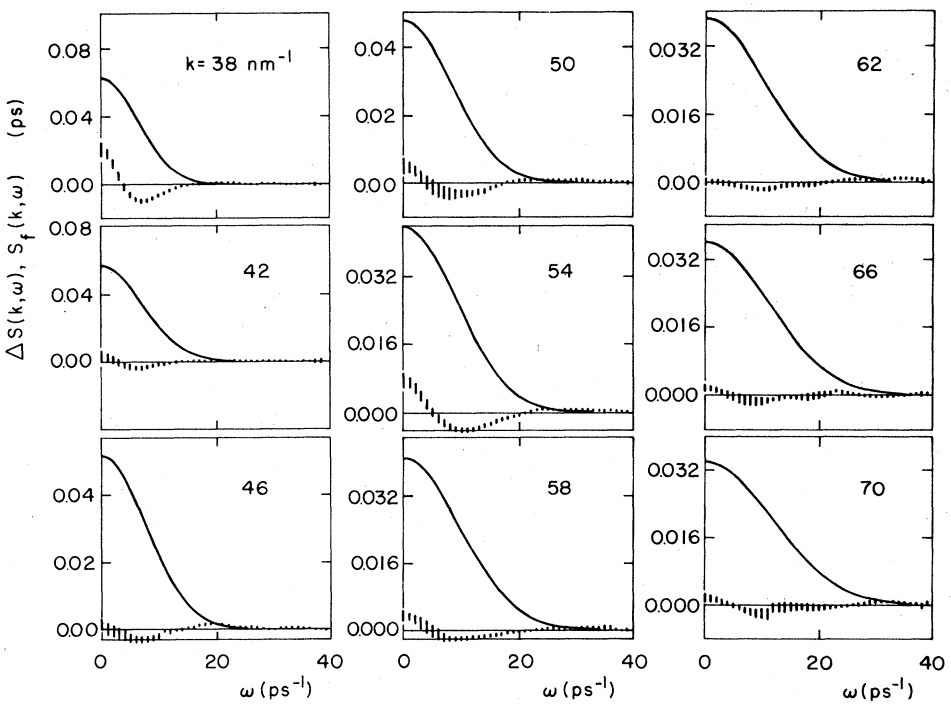

FIG. 6. $\Delta S(k,\omega)$ [defined by Eq. (11)] of measurement III, error bars; $S_f(k,\omega)$, solid line.

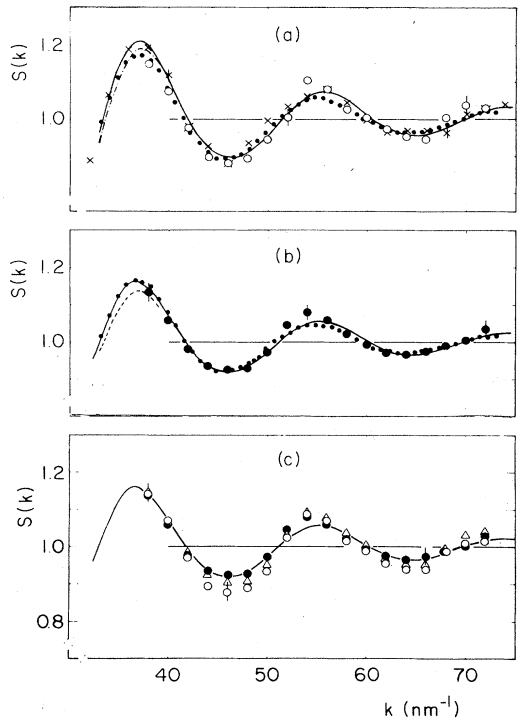

FIG. 7. Static structure factor as a function of k. For the meaning of the various acronyms, see Table III. (a) ○, Ar-III; —·—·—·, Ar-d; ×, CMD; •, Ne-c; —— MSA-III. (b) ●, Ar-I; — — —, Ar-a; •, Ne-a; ——, MSA-I. (c) ●, Ar-I; △, Ar-II; ○, Ar-III; ——, MSA-I. Note that the horizontal scale represents the wave number k of argon. The abscissa of the neon and LJ results are transformed conformably, using the LJ length parameters σ given in the text.

tures and densities of the experiments and calculations appearing in Fig. 7 are listed in Table III. We conclude that the MSA gives a good description of the experimental $S(k)$ and that the principle of corresponding states is valid for $S(k)$. Within the estimated uncertainties the quantum corrections to $S(k)$, which are expected to be more important in the case of neon and at larger k values,[19] appear to be too small to be detected.

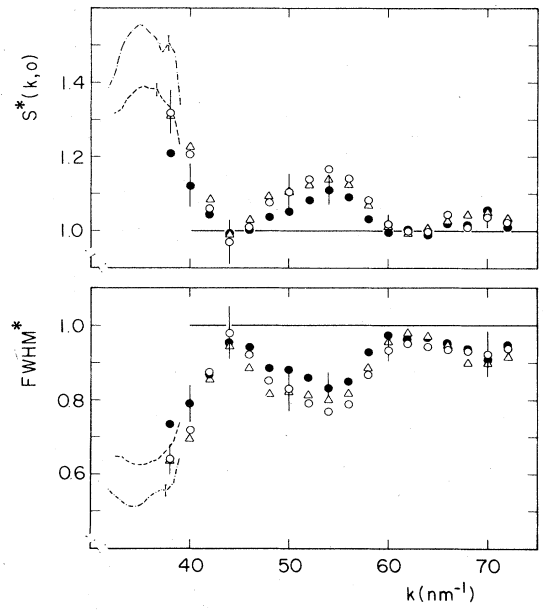

FIG. 8. Reduced peak height $S^*(k,0) = \tilde{S}(k,0)[S(k)S_f(k,0)]^{-1}$ and width $\omega^*_{1/2}(k) = \omega_{1/2}(k)/\omega_{1/2,f}(k)$ (denoted here as FWHM*) of the symmetrized dynamic structure factor. ●, Ar-I; △, Ar-II; ○, Ar-III; — — —, Ar-a; —·—·—·, Ar-d.

Besides $S(k)$, four other quantities will be used to characterize the experimental $\tilde{S}(k,\omega)$, viz., the peak height and full width at half maximum (FWHM) of $\tilde{S}(k,\omega)$, denoted by $\omega_{1/2}(k)$, and the peak position and peak height of the longitudinal current correlation function $\tilde{C}_l(k,\omega) = \omega^2 \tilde{S}(k,\omega)/k^2$.

In Fig. 8 the peak height divided by the experimental $S(k)$ and the free-gas value,

$$S^*(k,0) = \tilde{S}(k,0)[S(k)S_f(k,0)]^{-1} ,$$

and the width divided by its free-gas value

$$\omega^*_{1/2}(k) = \omega_{1/2}(k)/\omega_{1/2,f}(k)$$

are shown. With increasing k, $S^*(k,0)$ and $\omega^*_{1/2}(k)$ ap-

TABLE III. Measurements, simulation, and calculations.

Acronym	Source	n^* [a]	T^* [a]	Figure	Symbol
Ar-I	INS, present measurement I	0.667	0.973	3(b),7,8,9	●
Ar-II	INS, present measurement II	0.739	0.974	3(b),7,8,9	△
Ar-III	INS, present measurement III	0.764	0.974	3(b),7,8,9,12,13,14	○
Ar-a	INS, measurement a of Ref. 2	0.668	0.974	7,8,9	— — —
Ar-d	INS, measurement d of Ref. 2	0.763	0.974	7,8,9	—·—·—·
Ne-a	ND, measurement a of Ref. 14	0.688	0.968	7	•
Ne-c	ND, measurement c of Ref. 14	0.753	0.968	7	•
CMD	Present simulation	0.736	0.961	7,12,13	×
MSA-I	Present calculation[b]	0.667	0.974	7	——
MSA-III	Present calculation[b]	0.764	0.974	7	——

[a] $n^* = n\sigma^3$ and $T^* = k_B T/\varepsilon$, with LJ parameters (Ref. 12) $\sigma = 0.336$ (0.279) nm and $\varepsilon/k_B = 123.2$ (36.2) K for argon (neon).
[b] Calculated for a LJ system according to Ref. 13.

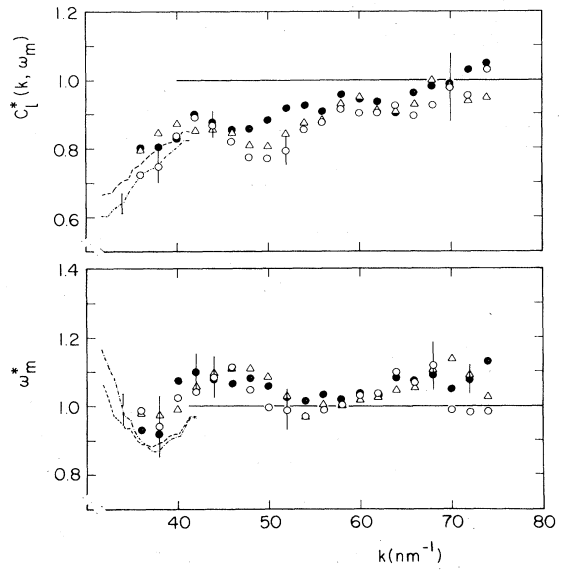

FIG. 9. Reduced peak position $\omega_m^*=\omega/\omega_{m,f}$ and peak height $C_l^*(k,\omega)=\tilde{C}_l(k,\omega_m)/C_{l,f}(k,\omega_{m,f})$ of the longitudinal current correlation function. Key as in Fig. 8.

proach unity from above and from below, respectively, both oscillating with the same period as $S(k)$. For both quantities the deviations from the free-gas limit decrease with decreasing density.

Figure 9 displays the peak position ω_m (Ref. 20) and peak height of $\tilde{C}_l(k,\omega)$, divided by their free-gas values, denoted by $\omega_m^*=\omega_m/\omega_{m,f}$ and $C_l^*(k,\omega_m)=\tilde{C}_l(k,\omega_m)/C_{l,f}(k,\omega_{m,f})$, respectively. Note that $S_f(k,0)$ and $C_{l,f}(k,\omega_{m,f})$ are proportional to k^{-1}, and $\omega_{1/2,f}(k)$ and $\omega_{m,f}$ to k.

IV. COMPARISON WITH THEORY

A. Classical system

The Gram-Charlier series expansion of $\tilde{S}(k,\omega)$ is given by[3–6]

$$\tilde{S}(k,\omega)=(2\pi)^{-1/2}(uk)^{-1}e^{-x^2}\sum_{n=0}^{\infty}\epsilon_n(k)H_n(x)\ , \qquad (12)$$

where $x^2=\frac{1}{2}\omega^2(uk)^{-2}$ and the Hermite polynomials $H_n(x)$ are defined by

$$H_n(x)=(-\tfrac{1}{2})^n e^{x^2}\frac{d^n}{dx^n}e^{-x^2}\ , \qquad (13)$$

yielding $H_0(x)=1$, $H_1(x)=x$, $H_2(x)=x^2-\frac{1}{2}$, $H_3(x)=x^3-\frac{3}{2}x$, and $H_4(x)=x^4-3x^2+\frac{3}{4}$. For a classical system, all ϵ_n with n odd vanish, $u^2=(\beta M)^{-1}$, and ϵ_n for $n=0$, 2, and 4 are given by

$$\epsilon_0(k)=S(k),\quad \epsilon_2(k)=1-S(k)\ ,$$
$$\epsilon_4(k)=\tfrac{1}{2}[S(k)-1]+\frac{\beta M}{6k^2}[\Omega^2(0)-\Omega^2(k)]\ , \qquad (14)$$

with

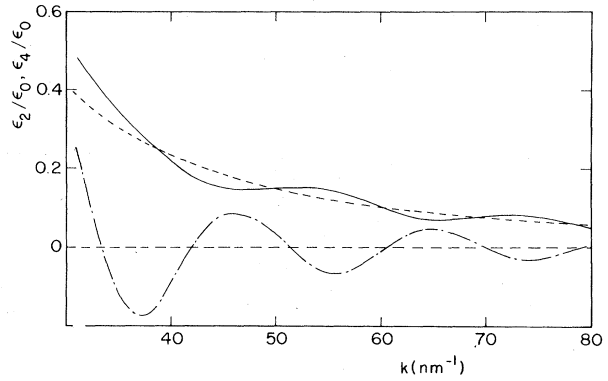

FIG. 10. Parameters in the Gram-Charlier expansion of $S(k,\omega)$, calculated according to MSA-III (Table III). ϵ_2/ϵ_0, dash-dotted line; ϵ_4/ϵ_0, solid line; corresponding values of $S_s(k,\omega)$, dashed lines.

$$\Omega^2(k)=\frac{n}{M}\int g(r)\cos(kz)\frac{d^2\varphi(r)}{dz^2}d\mathbf{r}\ .$$

Here we have assumed a pairwise additive interaction potential $\varphi(r)$. If only the self part of $S(k,\omega)$, $S_s(k,\omega)$, is considered, Eqs. (12) and (13) hold with

$$\epsilon_0(k)=1\ ,\quad \epsilon_2(k)=0\ ,$$
$$\epsilon_4(k)=\frac{k_4^2}{k^2}=\frac{\beta M\Omega^2(0)}{6k^2}\ . \qquad (15)$$

Numerical values for the parameter k_4 (Ref. 21) are given in Table II. If the series is truncated after the fourth-order term ($\epsilon_4 H_4$), Eq. (15) gives the first-order deviation from the free-gas limit in the exact large-k expansion of $S_s(k,\omega)$ for a classical system.[4] Figure 10 shows ϵ_2/ϵ_0 and ϵ_4/ϵ_0, calculated according to the MSA,[13] condition MSA-III (Table III), both for $S(k,\omega)$ and $S_s(k,\omega)$.

If a system with a continuous pair potential $\varphi(r)$ is considered, then, as $r\to 0$, $g(r)$ becomes asymptotically proportional to $\exp[-\varphi(r)]$.[22] Benfatto *et al.*[23] have shown that if $\varphi(r)$ decays at large r as a power law $\varphi(r)\sim r^{-m}$ with $m>3$ then, as $r\to\infty$, $g(r)-1$ becomes asymptotically proportional to $-\varphi(r)$. Making use of these limits, integration by parts readily shows that the oscillations of $S(k)-1$ and $\Omega^2(k)$ will decay to zero faster than any power of $1/k$. So, at large k the term of ϵ_4/ϵ_0 containing $\Omega^2(0)k^{-2}$ will then dominate, and $S(k,\omega)$ will approach $S_f(k,\omega)$ via $S_s(k,\omega)$.

The quantities given in Fig. 10 together with the MSA $S(k)$ were used to calculate $S(k,\omega)$ from Eq. (12), truncated after the $n=4$ term. $\Delta S(k,\omega)$, defined by Eq. (11), from this model is displayed for three k values in Fig. 11. The qualitative agreement between model (Fig. 11) and experiment (Fig. 6) is satisfactory.

In the following a quantitative comparison is made of the quantities $\tilde{S}(k,0)$, $\omega_{1/2}(k)$, ω_m, and $\tilde{C}_l(k,\omega_m)$ determined from experiment, theory, and CMD results. The CMD simulations were performed for a LJ system at $T^*=0.961$ and $n^*=0.736$ for a system of 864 particles, and the system has been followed during 89 000 time steps

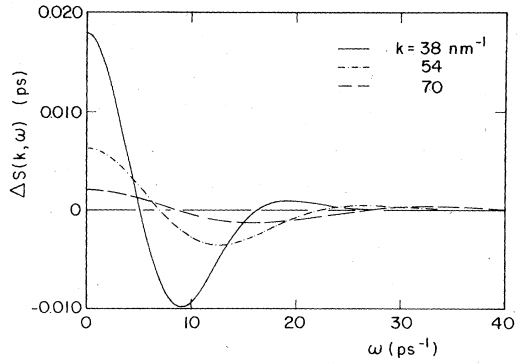

FIG. 11. $\Delta S(k,\omega)$ [defined by Eq. (11)] calculated with the Gram-Charlier expansion, truncated after the $n=4$ term, with parameters of Fig. 10.

of $\Delta\tau=0.005$ (corresponding to $\Delta t=0.01$ ps). Figure 12 shows $S^*(k,0)$ and $\omega^*_{1/2}(k)$. The dashed lines indicate the first-order corrections of $S_s(k,\omega)$ to the free-gas limit (Appendix B),

$$S^*_s(k,0)=1+\tfrac{3}{4}k^2_4k^{-2}+O(k^{-4})\,,$$
$$\omega^*_{1/2,s}(k)=1+\tfrac{1}{2}(\ln 2-3)k^2_4k^{-2}+O(k^{-4})\,. \tag{16}$$

In Fig. 13 ω^*_m and $C^*_l(k,\omega_m)$ are displayed. The first-order corrections (Appendix B) are given by

$$\omega^*_{m,s}(k)=1-\tfrac{1}{2}k^2_4k^{-2}+O(k^{-4})\,,$$
$$C^*_{l,s}(k,\omega_m)=1-\tfrac{5}{4}k^2_4k^{-2}+O(k^{-4})\,. \tag{17}$$

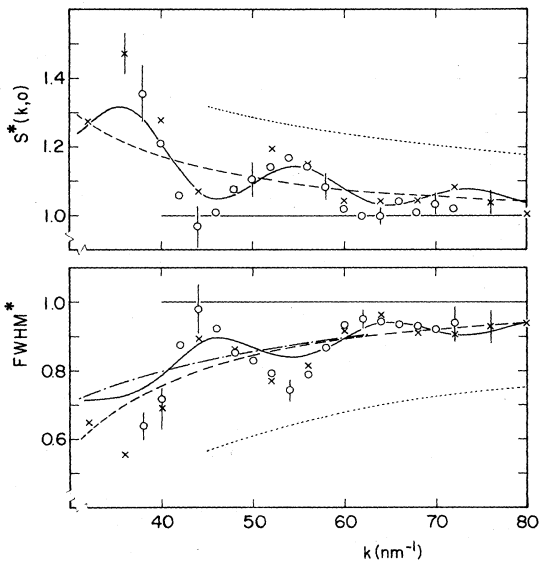

FIG. 12. $S^*(k,0)$ and $\omega^*_{1/2}(k)$ (denoted here as FWHM*) as a function of k. Ar-III, open circles; CMD, crosses; GC expansion (MSA-III) up to $n=4$, for $S(k,\omega)$, solid line, and for $S_s(k,\omega)$, dash-dotted line. First-order correction to $S_f(k,\omega)$ for a LJ system [Eq. (16)], dashed line [for $S^*(k,0)$ coincident with GC expansion], and for a HS system [Eqs. (18) and (19)], dotted line.

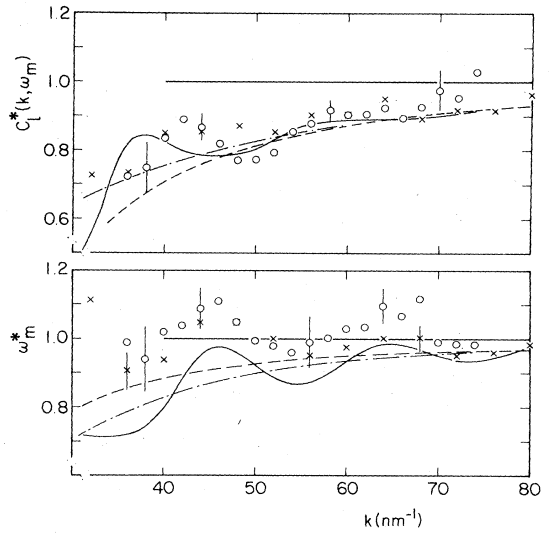

FIG. 13. $C^*_l(k,\omega_m)$ and ω^*_m as a function of k. Key as in Fig. 12.

It appears that for $k\gtrsim 3k_4$ (for this condition $k_4=19.3$ nm^{-1}), and within the estimated uncertainties, the experimental and CMD results for all four quantities are in good agreement with the theoretical large-k description. With decreasing k, the first four terms of the GC expansion are insufficient to yield a quantitative agreement. Concerning the quantities $S^*(k,0)$ and $\omega^*_{1/2}(k)$, this model underestimates the amplitude of the oscillations, while the oscillations in $C^*_l(k,\omega_m)$ given by the model are not in phase with the experimental and CMD results. Whereas, with decreasing k, ω^*_m both from the experiment and from CMD oscillates around a curve which has a tendency to increase and becomes larger than unity (see also Fig. 17 in Ref. 2), ω^*_m from the model oscillates around a decreasing curve.

Sears[4] pointed out that for a hard-sphere system the first correction term describing the FWHM of $S_s(k,\omega)$ at large k is proportional to k^{-1} [in contrast to the k^{-2} correction for a system with a continuous interaction potential, Eq. (16)],

$$\omega^*_{1/2,\mathrm{HS}}(k)=1+a_{\mathrm{HS}}(kl_E)^{-1}+O((kl_E)^{-2})\,, \tag{18}$$

where $l_E=[\pi\sqrt{2}nd^2g_{\mathrm{HS}}(d)]^{-1}$ is the Enskog mean free path, d the hard-sphere diameter, and $g_{\mathrm{HS}}(d)$ the pair correlation function for hard spheres at contact.[24] Sears[4] approximated $a_{\mathrm{HS}}\approx -0.27$. Recently, de Schepper *et al.*[25] derived exact expressions for $\omega^*_{1/2,\mathrm{HS}}(k)$, given by Eq. (18), and for $S^*_{\mathrm{HS}}(k,0)$,

$$S^*_{\mathrm{HS}}(k,0)=1+b_{\mathrm{HS}}(kl_E)^{-1}+O((kl_E)^{-2})\,, \tag{19}$$

where $a_{\mathrm{HS}}=-0.449$ and $b_{\mathrm{HS}}=0.328$. Using $d=0.343$ nm (Ref. 2) yields $g_{\mathrm{HS}}(d)=4.13$ and $l_E=0.023$ nm for condition III. The resulting first-order correction is indicated in Fig. 12. From this it is apparent that a representation of liquid argon by a hard-spheres system, which was shown to yield qualitatively good description in the

region $5 \lesssim kd \lesssim 15$,[26] fails to describe the larger-k behavior of $S(k,\omega)$.

B. Quantum system

We now go back to the measured—not symmetrized—dynamic structure factor $S(k,\omega)$, as shown in Fig. 5(a), and study its deviation from the large-k limit $S_{IA}(k,\omega)$ [which is, to order $\hbar^2$, given by Eq. (7), replacing v_0 by u of Eq. (8)], displayed in Fig. 5(b).

For a quantum system $S(k,\omega)$ can also be described by a GC expansion,[5,6] which yields, if only quantum corrections up to order $\hbar^2$ are considered, Eq. (12) with[21]

$$
\begin{aligned}
&x^2=\tfrac{1}{2}(\omega-\omega_R)^2(uk)^{-2}\,,\\
&\epsilon_0(k)=S(k)\,,\quad \epsilon_1(k)=-\frac{k}{k_1}\gamma(k)\,,\\
&\epsilon_2(k)=\left[\frac{1}{2}\left[\frac{k}{k_1}\right]^2-1\right]\gamma(k)+\frac{k_3}{2k_1}\mu(k)\,,\\
&\epsilon_3(k)=\frac{k}{k_1}\gamma(k)+\frac{k_3}{k}[1+\mu(k)]\,,\\
&\epsilon_4(k)=\frac{1}{2}\left[1-\left[\frac{k}{k_1}\right]^2\right]\gamma(k)\\
&\qquad+\left[\frac{k_4}{k}\right]^2[1+\mu(k)]+O(\hbar^2)\,,
\end{aligned}
\tag{20}
$$

where

$$
\begin{aligned}
&\gamma(k)=S(k)-1\,,\\
&\hbar k_1=Mu\sqrt{2}\,,\\
&k_3=\hbar\beta(2\beta M)^{1/2}\Omega^2(0)/6\,,
\end{aligned}
$$

and

$$
\mu(k)=-\Omega^2(k)/\Omega^2(0)+O(\hbar^2)\,.
$$

Numerical values of k_1, k_3, and k_4 for the present conditions are given in Table II.

The peak position, at fixed k, of $S(k,\omega)$ is denoted by $\omega_p(k)$. Figure 5(a) already indicated that ω_p lies in between $\omega=0$ and ω_R. Experimental results of ω_p/ω_R for Ar-III are shown in Fig. 14 as a function of k. In this graph we also display ω_p determined for $S(k,\omega)$ calculated according to Eq. (20), where $\mu(k)$ was approximated by the MSA value for a classical system.

For the self part $S_s(k,\omega)$ $\gamma(k)=\mu(k)=0$, yielding

$$
S_s(k,\omega)=(2\pi)^{1/2}(uk)^{-1}e^{-x^2}\left[1+\frac{k_3}{k}H_3(x)+O(k^{-2})\right]\,.
$$

The peak position of $S_s(k,\omega)$ is then given by

$$
\omega_p-\omega_R=uk\sqrt{2}\left[-\frac{3}{4}\frac{k_3}{k}+O(k^{-2})\right]\,,
$$

or

$$
\frac{\omega_p}{\omega_R}=1-\frac{\Omega^2(0)}{2u^2}k^{-2}+O(k^{-3})\,. \tag{21}
$$

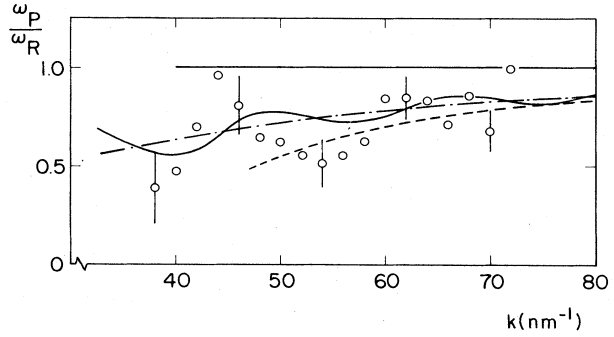

FIG. 14. Peak position ω_p of $S(k,\omega)$, divided by the recoil frequency ω_R, as a function of k. Ar-III, open circles; GC expansion (MSA-III) of $S(k,\omega)$ [Eq. (20)], solid line; and of $S_s(k,\omega)$, dash-dotted line; first-order correction to $S_{IA}(k,\omega)$ [Eq. (21)], dashed line.

The first-order correction in Eq. (21) is indicated in Fig. 14 by the dashed line.

It is shown that for $k \lesssim 60$ nm^{-1}, discrepancies between the experimental and theoretical results, both in the amplitude and the phase of the oscillations, become apparent, probably as a result of truncating the GC series after the $n=4$ term.

V. SUMMARY AND CONCLUSIONS

We reported inelastic neutron scattering data of liquid ^{36}Ar at pressures of 2, 27, and 40 MPa along the 120-K isotherm. The wave-number range covered by the experiment was $38<k<72$ nm^{-1}, enabling us to study the transition of $S(k,\omega)$ to its free-gas behavior [denoted $S_f(k,\omega)$]. Since an exact large-k expansion of $S_s(k,\omega)$ exists for a classical system, and since argon may be considered an "almost classical" system, the main objective of our study was the comparison between the quasiclassical approximation, $\tilde{S}(k,\omega)$, of the experimental $S(k,\omega)$ and the theory.

Sears[4] derived a large-k expansion of $S_s(k,\omega)$ for a system with a smooth interaction potential. From this we calculated for a LJ system the leading correction (of order k^{-2}) to the free-gas expression of the quantities $S_s(k,0)$, $\omega_{1/2,s}(k)$, $\omega_{m,s}$ and $C_{l,s}(k,\omega_m)$ and compared these with the experimental results. Except for ω_m, the experimental values oscillate around the theoretical first-order correction in the whole experimental k range, approaching it with increasing k. Due to experimental difficulties (see Sec. II), some systematic deviations might be present in the large-ω data, which could affect the experimental ω_m and $\tilde{C}_l(k,\omega)$ values. In order to check this, CMD simulations were performed. It appeared that, within the estimated uncertainties, the CMD results were in agreement with the experimental results. From both sets of data it was shown that at relatively large-k values ($k \gtrsim 70$ nm^{-1}) ω_m approaches the leading correction to the free-gas limit.

For a hard-sphere system the first correction to $S_f(k,\omega)$ is proportional to k^{-1} rather than to k^{-2}. From the present data we conclude that the large-k behavior of

$S(k,\omega)$ in liquid argon cannot be described by the hard-sphere expressions, this in contrast with H_2 gas[5,25(b)] and liquid sodium.[27,25(b)] The validity of the hard-sphere approximation of the H_2 gas may be understood by the fact that the experiments were performed at temperatures [85 and 300 K in Refs. 5 and 25(b), respectively] large compared with the depth of the potential well, which is equal to $\varepsilon/k_B \mp 36.7$ K.[28] Why the hard-sphere description seems to be valid for liquid sodium and not for liquid argon, while, in contrast, the repulsive part of the interaction potential of the former is softer,[29] is not yet understood.

The Gram-Charlier expansion of the coherent $S(k,\omega)$, truncated after the fourth-order term, and calculated for a LJ system, gives a qualitatively good description of the experimental $\tilde{S}(k,\omega)$ in the examined k range, going over into quantitative agreement with increasing k. In a future publication we will compare the present calculations with experimentally determined $S_s(k,\omega)$ data.

Because of the limited statistical accuracy of the present data no reliable fits could be obtained of a sum of three, or more, (extended heat and sound) eigenmodes.[30]

ACKNOWLEDGMENTS

It is a pleasure for us to thank I. M. de Schepper, H. Fredrikze, and P. Verkerk for the many fruitful discussions. We are indebted to B. J. M. Vernooy and A. J. W. Bouwman for their assistance during the course of the experiments, and to J. C. van Rijs and C. Bruin, who performed the computer molecular-dynamics simulations. The critical comments on the manuscript by J. J. van Loef are gratefully acknowledged.

APPENDIX A: DETAILS OF SOME CORRECTIONS

The inelastic scattering from the vanadium sample was approximated by the double differential cross section for incoherent one-phonon scattering.[31] We used the normalized vibrational density of states $Z(\omega)$ as determined in Ref. 2. At each scattering angle, the calculated intensity was broadened by the proper TOF resolution and normalized in such a way as to accomplish the best fit in the range from channel number 130 to 220 (see Fig. 15). Subtraction of the inelastic scattering resulted in a negative spectral intensity at the higher channel numbers, which was corrected for by adding a constant level to the spectrum.

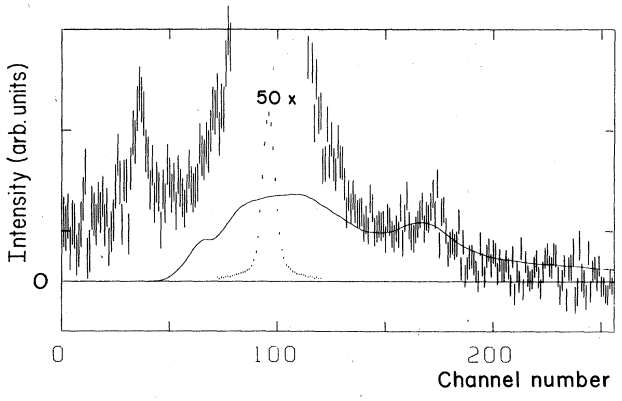

FIG. 15. Correction of the vanadium spectra for inelastic scattering (see text). TOF spectrum of vanadium at the scattering angle $\varphi = 89.3°$, error bars; calculated inelastic scattering, solid line.

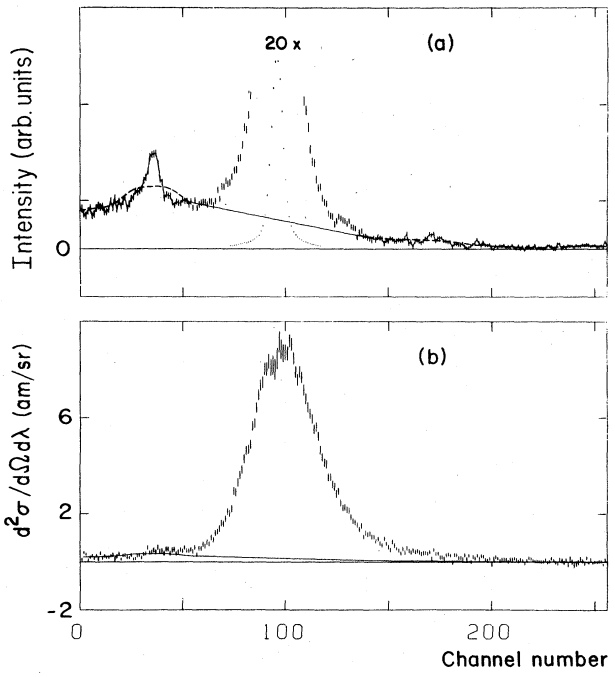

FIG. 16. Correction for parasitic reflections by the PG monochromator (see text). (a) Vanadium TOF spectrum summed over all scattering angles after subtraction of inelastic scattering, error bars; approximated intensity due to neutrons originating from parasitic PG reflections, and scattered by vanadium, continuous line; same, scattered by argon, dashed line. (b) Normalized ^{36}Ar TOF spectrum at the scattering angle $\varphi = 89.3°$, error bars; scattering due to parasitic PG reflections, solid line [the same as the dashed line in (a)].

The structure in the spectra left after this correction is due to the, not completely suppressed, parasitic reflections from the PG monochromator, mainly due to double Bragg[32] scattering and inelastic scattering. Since this intensity also distorted the argon spectra the latter were corrected for it in an approximate way. All vanadium spectra were summed and the intensity from the parasitic reflections was approximated by the solid line in Fig. 16(a). This intensity was convoluted by a rectangular function with a width which represented the broadening by the argon scattering, resulting in the dashed line. The curve thus obtained was, at each scattering angle, fitted to the argon spectra in the range from channel number 1 to 40 [an example is given in Fig. 16(b)] and then subtracted.

APPENDIX B: LARGE-k BEHAVIOR OF $S_s(k,\omega)$ FOR A CLASSICAL SYSTEM

Sears[4] has shown for an isotropic classical system with a smooth and velocity-independent interatomic potential that the larg-k behavior of the self part of the dynamic structure factor is given by

$$S_s(k,\omega)=S_f(k,\omega)[1+k_4^2H_4(x)k^{-2}+O(k^{-4})]\ , \tag{B1}$$

with

$$k_4^2=\beta M\Omega^2(0)/6\ ,$$
$$H_4(x)=x^4-3x^2+\tfrac{3}{4}\ ,\quad x^2=\tfrac{1}{2}\omega^2(uk)^{-2}\ ,$$
$$u^2=(\beta M)^{-1}\ ,$$

and the free-gas limit $S_f(k,\omega)=(2\pi)^{-1/2}(uk)^{-1}e^{-x^2}$.

In this appendix we will derive the leading term that describes the approach to the free-gas limit of the peak height and the FWHM of $S_s(k,\omega)$ $[\omega_{1/2,s}(k)]$ and of the peak position and peak height of $C_{l,s}(k,\omega)=\omega^2S_s(k,\omega)/k^2$. We will consider the function

$$S(x)=e^{-x^2}[1+\delta(x^4-3x^2+\tfrac{3}{4})]\ , \tag{B2}$$

where e^{-x^2} represents the free-gas limit and $\delta=(k_4/k)^2$ is the small parameter in the expansions below. The four quantities mentioned will be successively discussed and the subscript s will be omitted in the remainder of this appendix.

(i) The peak height is readily given by

$$S(0)=1+\tfrac{3}{4}\delta\ ,$$

yielding [with $S(k)=1$]

$$S^*(k,0)=S(k,0)/S_f(k,0)$$
$$=1+\tfrac{3}{4}k_4^2k^{-2}+O(k^{-4})\ . \tag{B3}$$

(ii) The half-width at half maximum (HWHM) x_h is given by $S(x_h)=\frac{1}{2}S(0)$ or

$$e^{-z}[1+\delta(z^2-3z+\tfrac{3}{4})]=\tfrac{1}{2}(1+\tfrac{3}{4}\delta)\ , \tag{B4}$$

where $z=x_h^2$ is a function of δ. If we represent the HWHM of the free-gas limit by z_0 then $e^{-z_0}=\frac{1}{2}$ and $z_0=\ln 2$. A Taylor-series expansion of z around z_0 yields

$$z=z_0+\delta\left[\frac{\partial z}{\partial\delta}\right]_{\delta=0}+O(\delta^2)\ . \tag{B5}$$

Differentiating Eq. (B4) with respect to δ and inserting $\delta=0$, $z=z_0$, and $e^{-z_0}=\frac{1}{2}$ yields

$$\left[\frac{\partial z}{\partial\delta}\right]_{\delta=0}=z_0(z_0-3)\ . \tag{B6}$$

Equations (B5) and (B6) give

$$z/z_0=1+(z_0-3)\delta+O(\delta^2)\ ,$$

or

$$\omega_{1/2}^*(k)=\frac{\omega_{1/2}(k)}{\omega_{1/2,f}(k)}=\left[\frac{z}{z_0}\right]^{1/2}$$
$$=1+\tfrac{1}{2}(\ln 2-3)k_4^2k^{-2}+O(k^{-4})\ , \tag{B7}$$

as was already obtained by Sears.[4]

(iii) The peak position x_m of $x^2S(x)$ is determined by the solution of

$$\frac{\partial}{\partial x}[x^2S(x)]\,|_{x=x_m}=0\ .$$

In the free-gas limit, the peak position of $x^2e^{-x^2}$ is given by $x_0=1$. If we define $z=x^2$, then $\partial/\partial x=2x\,\partial/\partial z$, and $z_m=x_m^2$ is determined by the solution of

$$\frac{\partial}{\partial z}[zS(z)]\,|_{z=x_m^2}=0\ . \tag{B8}$$

A Taylor-series expansion around $z_0=x_0^2=1$ yields

$$z_m=z_0+\delta\left[\frac{\partial z_m}{\partial\delta}\right]_{\delta=0}+O(\delta^2)\ . \tag{B9}$$

Equation (B8) together with Eq. (B2) gives

$$\delta(-z_m^3+6z_m^2-\tfrac{27}{4}z_m+\tfrac{3}{4})-z_m+1=0\ . \tag{B10}$$

Differentiating Eq. (B10) with respect to δ and inserting $\delta=0$ and $z_m=z_0^2=1$ yields

$$\left[\frac{\partial z_m}{\partial\delta}\right]_{\delta=0}=-1\ . \tag{B11}$$

Equations (B9) and (B11) give

$$z_m=z_0(1-\delta)+O(\delta^2)\ ,$$

or

$$\omega_m^*=\frac{\omega_m}{\omega_{m,f}}=\left[\frac{z_m}{z_0}\right]^{1/2}=1-\tfrac{1}{2}k_4^2k^{-2}+O(k^{-4})\ . \tag{B12}$$

(iv) The peak height of $C_l(k,\omega)$ is proportional to

$$z_mS(z_m)=z_me^{-z_m}[1+\delta(z_m^2-3z_m+\tfrac{3}{4})]\ . \tag{B13}$$

Using $z_m=z_0(1-\delta)+O(\delta^2)$ gives

$$e^{-z_m}=e^{-z_0}[1+z_0\delta+O(\delta^2)]\ . \tag{B14}$$

If we furthermore use that, to first order in δ, $\delta f(z_m)=\delta f(z_0)$ and $z_0=1$, then

$$z_mS(z_m)=z_0(1-\delta)(1+\delta)e^{-z_0}(1-\tfrac{5}{4}\delta)\ , \tag{B15}$$

leading to

$$C_l^*(k,\omega_m)=\frac{C_l(k,\omega_m)}{C_{l,f}(k,\omega_{m,f})}$$
$$=\frac{z_mS(z_m)}{z_0S(z_0)}=1-\tfrac{5}{4}k_4^2k^{-2}+O(k^{-4})\ . \tag{B16}$$

[1]P. Verkerk, *Neutron Inelastic Scattering 1977* (IAEA, Vienna, 1978), Vol. II, p. 53; P. Verkerk, Ph.D. thesis, University of Technology, Delft (1985); P. Verkerk and A. A. van Well (unpublished).

[2]A. A. van Well, P. Verkerk, L. A. de Graaf, J.-B. Suck, and J. R. D. Copley, Phys. Rev. A **31**, 3391 (1985).

[3]B. R. A. Nijboer and A. Rahman, Physica **32**, 415 (1966).

[4]V. F. Sears, Phys. Rev. A **5**, 452 (1972).

[5]V. F. Sears, Phys. Rev. A **7**, 340 (1973).

[6]V. F. Sears, Phys. Rev. **185**, 200 (1969); Phys. Rev. A **1**, 1699 (1970).

[7]*Neutron Beam Facilities in Western Europe,* edited by J. Joffrin (European Science Foundation, Strassbourg, 1981).

[8]P. Verkerk and A. M. M. Pruisken, Nucl. Instrum. Methods **160**, 439 (1979).

[9]R. B. Stewart, R. T. Jacobsen, J. H. Becker, J. C. J. Teng, and P. K. K. Mui, in *Proceedings of the Eighth Symposium on Thermophysical Properties,* edited by J. V. Sengers (ASME, New York, 1982), p. 97.

[10]M. Kamal, S. S. Malik, and D. Rorer, Phys. Rev. B **18**, 1609 (1978).

[11]P. Verkerk and A. A. van Well, Nucl. Instrum. Methods Phys. Res. A **228**, 438 (1985).

[12]J. Rouch, J. P. Boon, and P. A. Fleury, Physica A **88**, 347 (1977).

[13]W. G. Madden and S. A. Rice, J. Chem. Phys. **72**, 4208 (1980).

[14]L. A. de Graaf and B. Mozer, J. Chem. Phys. **55**, 4967 (1971).

[15]A. A. van Well and L. A. de Graaf, Interuniversitair Reactor Instituut (Delft) Report No. IRI-132-85-06, 1985, available on request (unpublished).

[16]K. S. Singwi and A. Sjölander, Phys. Rev. **120**, 1093 (1960); R. Aamodt, K. M. Case, M. Rosenbaum, and P. F. Zweifel, *ibid.* **126**, 1165 (1962).

[17]L. D. Landau and E. M. Lifshitz, *Statistical Physics* (Pergamon, London, 1959), p. 102.

[18]L. Verlet, Phys. Rev. **159**, 98 (1967).

[19]Both F. Barocchi, M. Neumann, and M. Zoppi, Phys. Rev. A **31**, 4015 (1985) and R. A. Young, Phys. Rev. A **23**, 1498 (1981) show that taking into account the quantum corrections to $S(k)$ results in a shift of the peaks to smaller k values. For the present conditions, the results from both references are consistent with a change of the k scale by 1%.

[20]The method of determining ω_m from INS data as described in Appendix B of Ref. 2 overestimates ω_m of the free-gas limit by 3%. The ω_m values presented here were determined by the same method and, since $S(k,\omega)$ is close to its free-gas limit, we corrected the obtained ω_m by 3%.

[21]For the parameters k_1, k_3, and k_4 appearing in the GC expansion we followed the notation introduced by Sears in Ref. 6.

[22]B. Widom, J. Chem. Phys. **39**, 2808 (1963).

[23]G. Benfatto, Ch. Gruber, and Ph. A. Martin, Helv. Phys. Acta **57**, 63 (1984).

[24]F. H. Ree and W. G. Hoover, J. Chem. Phys. **40**, 939 (1964).

[25](a) I. M. de Schepper, M. H. Ernst, and E. G. D. Cohen, J. Stat. Phys. **25**, 321 (1981); (b) W. Montfrooy, P. Verkerk, and I. M. de Schepper (unpublished).

[26]P. M. Furtado, G. F. Mazenko, and S. Yip, Phys. Rev. A **12**, 1653 (1975); **13**, 1641 (1976); I. M. de Schepper and E. G. D. Cohen, *ibid.* **22**, 287 (1980); I. M. de Schepper, E. G. D. Cohen, and M. J. Zuilhof, Phys. Lett. **101A**, 399 (1984).

[27]Ch. Morkel, Ph.D. thesis, Technische Universität, München (1984); W. Gläser and Ch. Morkel, J. Non-Cryst. Solids **61**, 309 (1980).

[28]A. M. Michels, W. de Graaf, and C. A. ten Seldam, Physica **26**, 393 (1960).

[29]S. K. Mitra, J. Phys. C **11**, 3551 (1978). In the region $r < \sigma$, the interaction potential is proportional to r^{-5}.

[30]I. M. de Schepper, P. Verkerk, A. A. van Well, and L. A. de Graaf, Phys. Rev. Lett. **50**, 974 (1983); E. G. D. Cohen, I. M. de Schepper, and M. J. Zuilhof, Physica B&C **127**, 282 (1984).

[31]S. W. Lovesey, *Theory of Neutron Scattering from Condensed Matter* (Clarendon, Oxford, 1984), Vol. I, p. 121.

[32]L. A. de Graaf, Interuniversitair Reactor Instituut (Delft) Report No. IRI-132-83-06, 1983 (unpublished), in Dutch. The sharp peak at channel 35 is due to 0.122-nm neutrons scattered from $(\bar{2}09)$ and (110) planes.